HHS Public Access

Author manuscript

Cancer Res. Author manuscript; available in PMC 2018 September 15.

Published in final edited form as:

Cancer Res. 2017 September 15; 77(18): 5142–5157. doi:10.1158/0008-5472.CAN-16-2586.

Cancer-Associated Fibroblasts Share Characteristics and Pro-tumorigenic Activity with Mesenchymal Stromal Cells

Lucia Borriello[1,2,6], **Rie Nakata**[1,2,6], **Michael A. Sheard**[1,2,6], **G. Esteban Fernandez**[6], **Richard Sposto**[1,2,3,6], **Jemily Malvar**[1,2,6], **Laurence Blavier**[1,2,6], **Hiroyuki Shimada**[4,6], **Shahab Asgharzadeh**[1,2,4,6], **Robert C. Seeger**[1,2,6], and **Yves A. DeClerck**[1,2,5,6]

[1]Division of Hematology, Oncology and Blood and Marrow Transplantation, Keck School of Medicine of the University of Southern California, Los Angeles, CA 90027

[2]Department of Pediatrics, Keck School of Medicine of the University of Southern California, Los Angeles, CA 90027

[3]Department of Preventive Medicine, Keck School of Medicine of the University of Southern California, Los Angeles, CA 90027

[4]Department of Pathology, Keck School of Medicine of the University of Southern California, Los Angeles, CA 90027

[5]Department of Biochemistry and Molecular Medicine, Keck School of Medicine of the University of Southern California, Los Angeles, CA 90027

[6]The Saban Research Institute, Children's Hospital Los Angeles, Los Angeles, CA 90027

Abstract

Cancer-associated fibroblasts (CAF) have been suggested to originate from mesenchymal stromal cells (MSC), but their relationship to MSC is not clear. Here we have isolated from primary human neuroblastoma (NB) tumors a population of αFAP- and FSP-1-expressing CAF that share phenotypic and functional characteristics with bone marrow-derived MSC (BM-MSC). Analysis of human NB tumors also confirmed the presence of αFAP- and FSP-1-positive cells in the tumor stroma, and their presence correlated with that of M2 tumor-associated macrophages. These cells (designated CAF-MSC) enhanced in vitro NB cell proliferation, survival, and resistance to chemotherapy and stimulated NB tumor engraftment and growth in immunodeficient mice, indicating an effect independent of the immune system. The pro-tumorigenic activity of MSC in vitro and in xenografted mice was dependent on the co-activation of JAK2/STAT3 and MEK/ERK1/2 in NB cells. In a mouse model of orthotopically implanted NB cells, inhibition of JAK2/STAT3 and MEK/ERK/1/2 by ruxolitinib and trametinib potentiated tumor response to etoposide and increased overall survival. These data point to a new type pro-tumorigenic CAF in the tumor microenvironment (TME) of NB and to STAT3 and ERK1/2 as mediators of their activity.

Corresponding Author: Yves A. DeClerck, Division of Hematology, Oncology, and Blood & Marrow Transplantation, Children's Hospital Los Angeles, 4650 Sunset Blvd, MS#54, Los Angeles, CA 90027. Phone: 323-361-2150; Fax: 323-361-4902; declerck@usc.edu.

Conflict of Interest Statement: None of the authors have a conflict of interest to declare.

Keywords

Cancer Associated Fibroblasts; Mesenchymal Stromal Cells; Tumor Microenvironment; Neuroblastoma; STAT3; ERK1/2

INTRODUCTION

The important contribution of the tumor microenvironment (TME) to cancer progression, metastasis and therapeutic resistance is well recognized (1). Endothelial cells (EC), innate and adaptive immune inflammatory cells and cancer-associated fibroblasts (CAF) all contribute to a TME that can promote the growth and dissemination of cancer cells (2). CAF represent a heterogeneous population of cells that have different functions depending on the tumor types (3). Like tumor-associated macrophages (TAM) (4), CAF can be polarized towards type I cells that display tumor-inhibitory activity, or type II cells that have tumor-promoting activity (5). In contrast to TAM, where markers of polarization have been well defined (4), markers in CAF have not been entirely elucidated (5). Thus, a better phenotypic and functional characterization of these cells is needed to understand their biological role.

The origin of CAF in tumors is also not entirely defined. Although they can originate from adjacent tissues, they can also derive from bone marrow (BM) cells (6,7). Mesenchymal stromal cells (MSC), which have the potential to differentiate into osteoblasts, adipocytes, and chondrocytes, are being recruited at the site of tissue injury where they contribute to tissue repair (8). In cancer, experiments in mice have suggested that BM-MSC can be recruited by primary tumors where they can transition into CAF (7,9,10).

To further investigate the relation between CAF and MSC in human cancer, we performed *in vitro* and *in vivo* comparative studies between CAF and BM-MSC obtained from patients with neuroblastoma (NB), the most common extracranial solid tumor in children (11) and a cancer where the role of the TME has been increasingly recognized (12). Our data identified a new population of CAF that is phenotypically and functionally similar to BM-MSC. We demonstrate that these cells exert broad pro-tumorigenic activities through the activation of the STAT3 and ERK1/2 signaling pathways in NB cells.

MATERIALS AND METHODS

Cell Culture

NB cell lines CHLA-255, SK-N-SH, SK-N-BE2 and CHLA-90 were initially obtained in 1998 from Dr. C. Patrick Reynolds (Texas Tech University Health Sciences Center, Lubbock, TX) and grown as previously described (13). Human skin fibroblasts (Fb) were purchased from American Type Culture Collection and cultured in Dulbecco's Modified Eagle's Medium (DMEM, Lonza) supplemented with 20% (v/v) heat-inactivated fetal bovine serum (FBS) and 1% penicillin/streptomycin (Gibco). All cell lines were authenticated at the beginning of the planned experiments by genotype analysis using the AmpFISTR Identifier PCR kit and GeneMapper ID v. 3.2 (Applied Biosystems) and tested negative for mycoplasma by MycoAlert™ mycoplasma detection kit from Lonza. CHLA-255 cells were used between passage 18 and 25 and authenticated in January 2013.

SK-N-SH cells were used between passage 41 and 50 and authenticated in January 2013. SK-N-BE(2) cells, passage 28 were authenticated in May 2014. CHLA-90 cells were used between passage 34 and 38 and authenticated in January 2013.

Isolation of CAF-MSC and BM-MSC from Primary Tumor and Bone Marrow of Patients

CAF-MSC were obtained from fresh NB tumor specimens from patients undergoing surgery at Children's Hospital Los Angeles (CHLA) and enrolled in the New Approaches to Neuroblastoma Therapy (NANT) Consortium Biorepository (N2004-05) or the CHLA Neural Tumor Registry protocols approved by the Institutional Review Board (IRB). Tumor tissues were washed with PBS, cut into small pieces and digested with 3 mg/ml collagenase I (Sigma) and 5 MU/ml of DNase I (Calbiochem) in PBS for 2 hours at 37°C. Cells were passed through a 70 μm strainer filter and negatively selected for GD2 expression. The collected cells were then plated in 100 mm dishes pre-coated with fibronectin (1 μg/ml; Calbiochem) and collagen I (3 μg/ml; Advanced BioMatrix) and cultured in DMEM supplemented with 20% FBS and 1% penicillin/streptomycin. After 15 days in culture, adherent cells were harvested, characterized as described below, and stored as frozen stock (passage 1). Cells were used between passages 2 and 8.

BM-MSC were obtained from fresh BM samples from patients with NB enrolled in the NANT Consortium Biorepository (N2004-05) or the CHLA Neural Tumor Registry protocols approved by the Children's Oncology Group and by the IRB at CHLA. The mononuclear cell fraction from the BM aspirate was isolated by Ficoll-Hypaque (Sigma) density gradient centrifugation at $400 \times g$ for 35 minutes. After three washes with PBS, mononuclear cells were plated in 100 mm dishes. After 15 days in culture, adherent cells were harvested, characterized and stored as frozen stock (passage 1).

Differentiation Assays

Adipogenesis, osteogenesis and chondrogenesis differentiation was performed as previously described (14) using specific differentiation media (StemPro, Gibco). Quantification of differentiated cells was performed by solubilization of Oil Red O in isopropanol, Alizarin Red in 10% acetic acid and Alcian Blue in 6M guanidine hydrochloride followed by OD measurement at A_{540}, A_{405} and A_{595} respectively.

Reagents

The antibodies used for flow cytometry, immunofluorescence, immunohistochemistry and Western blot are listed in Supplementary Table A. Etoposide (5 mg/ml in saline solution) was purchased from Teva Generics. Melphalan was purchased from Sigma-Aldrich and dissolved in acidified ethanol solution at a stock concentration of 64 mg/ml. Ruxolitinib was purchased from Selleckchem for *in vitro* studies and ruxolitinib phosphate salt was obtained from LC Laboratories for *in vivo* studies. Trametinib was purchased from LC Laboratories for *in vitro* and *in vivo* studies. Inhibitors were solubilized in DMSO at a stock concentration of 10 mM.

Flow Cytometry for Surface Expression Markers and Intracellular Signaling

CAF-MSC and BM-MSC were harvested with PBS-based cell dissociation buffer (Gibco) (1×10^5 cells per tube), washed, suspended in stain buffer (PBS with 5% (v/v) FBS and 0.1% (w/v) sodium azide), and stained with the fluorochrome-conjugated antibodies described in Supplementary Table A for 1 hour in the dark and in ice water. Nonspecific background signals were measured by incubating separate tubes with appropriate isotype-matched irrelevant antibodies. To compensate for the spillover of fluoresced light into unintended channels, other control tubes were stained with only one individual fluorochrome. Cells were washed twice with stain buffer, resuspended in 0.5 ml stain buffer, and filtered through a 40 μm mesh prior to flow cytometric data acquisition using an LSRII flow cytometer (BD Biosciences, San Jose, CA). For compensation, the AutoComp software routine in FACS Diva software (BD Biosciences) was employed. Cell debris and clumps were electronically gated from analysis based on their forward and side light scatter parameters. Data analysis was performed using FCS Express software (DeNovo Software, Los Angeles, CA). Mean fluorescence intensity (MFI) index was calculated as the ratio of MFI of stained cells with a specific antibody over MFI of cells stained with the isotype-matched control antibody.

For flow cytometry analysis of xenografts, tumors were harvested, cut into small pieces and digested with 10,000 collagenase digestion units (CDU)/ml of collagenase I (Sigma), 32 mg/ml of Dispase II (Roche) and 5 MU/ml of DNase I (Calbiochem) in PBS for 1 hour, and further dissociated using the gentleMACS Dissociator (Miltenyi Biotec). Resulting single cell suspensions were washed with PBS supplemented with 0.5% BSA and 2 mM EDTA, and filtered through a 70 μm nylon mesh. Cells were resuspended in stain buffer (PBS with 5% FBS and 0.1% sodium azide) and stained for GD2 using antibody and dilution described in Supplementary Table A for 30 minutes in the dark and ice water. Cells were then washed with PBS with 5% FBS and fixed using Fix Buffer I (BD Biosciences) for 30 minutes at 37°C. After fixation, cells were permeabilized using Perm Buffer III (BD Biosciences) for 30 minutes on ice and stained for p-STAT3 and p-ERK1/2 using antibodies and dilution described in Supplementary Table A for 30 minutes in the dark and ice water. Data analysis was performed using FCS Express software and the MFI was calculated as above.

Conditioned Medium

To generate conditioned media (CM), NB cells (4×10^6) were plated with CAF-MSC, BM-MSC or Fb (1×10^6) (ratio 4:1) in 100 mm dishes in 10 ml of culture medium supplemented with 10% FBS. As control, NB cell lines were cultured alone under the same conditions. After 48 hours, the CM was collected, centrifuged at $1{,}000\times g$ for 10 minutes at 4°C to eliminate floating cells and debris, and frozen at −80°C until used for experiments. For experiments, CM from frozen stock was diluted 1:1 with regular serum-free Iscove-Modified Dulbecco's medium (IMDM).

Cell Viability and Proliferation Assays

NB luciferase-labeled (NB-Fluc) cells were plated in triplicate in 96-well plates at a density of 10,000 cells per well together with either CAF-MSC, BM-MSC or Fb (2,500 cells per well; ratio 4:1), and cell viability was examined every 24 hours for a 96-hour period by adding D-luciferin (150 μg/ml; Biosynth) and measuring luciferase intensity with the Glo-

Max-Multi Detection System and Instinct software (Promega). Cell viability for non luciferase-expressing NB cells was assessed by adding CellTiter-Glo reagent (ratio 1:1) (Promega) to the medium according to the manufacturer's instructions. After 10 minutes, luminescence was measured via the Glo-Max-Multi Detection System (Promega). Data were calculated in Relative Luminescence Units (RLU).

For proliferation analysis, cells were plated in triplicate in 6-well plates at a density of 200,000 cells per well and treated with CM. After 48 hours of incubation at 37°C, cells were pulsed with bromodeoxyuridine (BrdU) for 40 minutes before being harvested and incubated in the presence of an FITC-conjugated anti-BrdU antibody, and 7-amino actinomycin D (7-AAD, BD Pharmingen) according to the manufacturer's instructions and then analyzed by flow cytometry using CellQuestPro software.

Apoptosis Assays

Cells were plated in triplicate in 6-well plates at a density of 200,000 cells per well and treated with the indicated concentrations of etoposide in the presence of CM for 48 hours. After treatment, detached and attached cells were collected together and apoptosis was analyzed using an Annexin V-FITC Apoptosis Detection Kit (BD Biosciences) according to the manufacturer's instructions and analyzed by flow cytometry using CellQuestPro software. Apoptotic cells included both early (Annexin V-positive and PI-negative) and late (Annexin V-positive and PI-positive) apoptotic cells. Alternatively, cells were plated in triplicate in 96-well plates at a density of 10,000 cells per well, treated with increasing concentrations of etoposide in the presence of CM, and incubated for 48 hours at 37°C. Apoptosis was measured as caspase 3/7 activity by adding Caspase-Glo 3/7 reagent (ApoLive-Glo Multiplex Assay; Promega) to the medium (ratio 1:1) and measuring luminescence using the Glo-Max-Multi Detection System (Promega).

PathScan Intracellular Signaling Array Kit and Western Blot

NB cells were exposed to CM from NB/CAF-MSC, NB/BM-MSC or NB/Fb co-cultures for 30 minutes, washed with ice-cold PBS, harvested and lysed in RIPA buffer supplemented with protease and phosphatase inhibitor cocktail (Thermo Scientific). The PathScan Intracellular Signaling Array Kit (Cell Signaling Technology #7744) was used according to the manufacturer's instructions. Proteins were detected by streptavidin-conjugated DyLight™ 680, and fluorescence images were captured using the Odyssey Infrared Imaging Systems (LI-COR Biosciences), and spot intensities were quantified using array analysis software (LI-COR Biosciences). Western blots were performed using standard protocols.

Cytokine Profiling Array

CM generated from NB cells (CHLA-255), CAF-MSC, BM-MSC, NB/CAF-MSC and NB/BM-MSC were examined for the presence of 36 different inflammatory markers using a Human Cytokine Array (R&D System ARY005B) according to the manufacturer's instructions. Briefly, membranes were incubated with 2 ml of CM and a cocktail of biotinylated antibodies overnight at 4°C. Following three washes, membranes were incubated in the presence of 2 ml (1:2000 dilution) of streptavidin-horseradish peroxidase (HRP) for 30 minutes at room temperature and the presence of immunocomplexes was

detected by staining with 3,3′-diaminobenzidine (DAB) chromogen. Arrays were scanned and pixel density measurements were obtained using the array analysis software of LI-COR Biosciences.

Immunofluorescence

CAF-MSC were seeded on sterilized glass coverslips overnight. Cells were then fixed in 4% (w/v) paraformaldehyde at room temperature for 10 minutes, washed with PBS, permeabilized with 0.1% (v/v) Triton X-100 for 10 minutes, blocked with 10% FBS at room temperature for 30 minutes and incubated overnight at 4°C in the presence of primary antibodies against αFAP, FSP-1 and αSMA described in Supplementary Table A. After washing in PBS, slides were incubated for 1 hour at room temperature with secondary antibodies conjugated with Alexa Fluor 488 and Phalloidin conjugated with Alexa Fluor 568 (Supplementary Table A). Following three washes in PBS, cells were embedded in VectaShield mounting medium with 4,6-diamidino-2-phenylindole (DAPI; Vector Laboratories). Fluorescence images were captured using an LSM 700 confocal system mounted on an AxioObserver.Z1 microscope equipped with a 20x/0.8 Plan-APOCHROMAT objective lens (Carl Zeiss Microscopy, Thornwood, NY).

Immunohistochemistry

Human paraffin-embedded sections (4 μm) of NB tumors were obtained through the Children's Oncology Group (COG) Biorepository by Dr. H. Shimada (COG study ANBL00B1). Informed consent was obtained from patient's parents or legal guardians by COG investigators. The study (PI; Dr Shimada) was approved by the CHLA institutional Review Board under number CCI-11-00261 (Neuroblastoma Pathology) and conducted under the U.S. Common Rule. Slides were deparaffinized in xylene and rehydrated in a graded series of ethanol solutions. Antigen unmasking was performed with 10 mM of sodium citrate (pH 6.0) for 3 cycles of 4 minutes each at 100°C. Slides were rinsed with PBS and incubated with 3% H_2O_2 for 10 minutes to block endogenous peroxidase activity, and blocked in 10% (v/v) goat serum in PBS for 1 hour at room temperature. Slides were then incubated overnight at 4°C with antibodies against αFAP and FSP-1 followed by one hour incubation at room temperature with the secondary antibody. After washing three times with 0.1% (v/v) Triton-X 100 in PBS, slides were incubated with biotin-free polymeric horseradish peroxidase (HRP) linker for 1 hour at room temperature, followed by washing with PBS and incubation with peroxidase-conjugated streptavidin for 30 minutes at room temperature. After washing with PBS, slides were stained with DAB chromogen and counterstained with hematoxylin. Negative controls included incubation with PBS solution instead of the primary antibody.

For the dual immunofluorescence on NB paraffin-embedded tissues, sections were sequentially incubated in the presence of a mouse anti-human FSP-1 and a rabbit anti-human CD163 using antibodies and dilution described in Supplementary Table A. After washing, the slides were incubated for 1 hour at room temperature with secondary antibodies conjugated with Alexa Fluor 488 and Alexa Fluor 594. The slides were mounted in DAPI containing Vectashield medium. Negative controls included incubation with PBS solution instead of the primary antibody.

Mouse paraffin-embedded sections (4 μm) of xenografted tumors were processed following the same protocol described above and stained for Ki-67 and FSP-1. DAB staining of the 20× digital images was quantified using Fiji ImageJ software (15). For the Ki-67 quantification, the brightness of each RGB TIFF image was normalized according to the brightest pixel. The nuclei were demarcated by converting the image to grayscale, applying an Unsharp Mask filter of radius 5 and weight 0.9, auto thresholding, and performing watershed segmentation. Each nucleus was classified as Ki-67-positive or Ki-67-negative according to the mean intensity in the L channel of the L·a·b color space in the brightness-normalized image; ambiguously stained nuclei were excluded from the count.

Xenograft Experiments

Animal experiments were performed under a protocol approved by the Institutional Animal Care and Use Committee at CHLA (Protocol #41-14 approved on November 7, 2014).

Subcutaneous implantation—CHLA-255-FLuc cells were injected either alone (4×10^6) or mixed with CAF-MSC, BM-MSC or Fb (1×10^6) in the flank of 6 week-old female and male NOD/SCID or NOD/SCID/IL-2Rγnull (NSG) mice. For CAF-MSC, 0.5, 1 and 2×10^6 cells were tested. Bioluminescent signals were measured by Xenogen imaging (Caliper Life Sciences), performed 15 minutes after intraperitoneal injection of D-luciferin (1.5 mg/mouse). Tumors were measured every three days using a vernier caliper, and tumor volume was calculated using the ellipsoid formula: tumor volume (mm^3) = (width in mm)^2 × (length in mm) × π/6. Mice were euthanized with O_2/CO_2 when tumors reached 1500 mm^3 or became ulcerated, or when animals were in distress (tumor ulceration, body weight loss above 20%, respiratory distress).

Orthotopic sub-renal capsule implantation—As an orthotopic model, we modified a model previously reported by us (16). Rather than implanting a fragment of a subcutaneous NB tumor in the adrenal gland, we injected NB cells and CAF-MSC under the renal capsule. This was needed as we could not inject a mixture of cells in suspension directly into the adrenal gland. This modification did not affect the growth, invasive and metastatic behavior of NB cells. In brief, 8–10 week-old female and male NSG mice were placed under general anesthesia, the left kidney was exteriorized and CHLA-255-FLuc cells alone (0.4×10^6) or mixed with CAF-MSC (0.1×10^6) were injected under the kidney capsule using a custom-made 50-μl glass syringe with a cemented 1.3-cm 30-gauge blunt needle. Following injection of the cells, the kidney was returned to the retroperitoneal space and muscle and skin were sealed. Animals were observed every day for signs of tumor growth (abdominal distension), local tumor invasion (leg palsy), weight loss, and distress. Tumor growth was monitored by bioluminescence as described above and by magnetic resonance imaging (MRI) using a 7.05 Pharmascan MRI (Bruker) after i.p. injection of 30μl of the contrast agent Magnevist (Bayer Pharmaceuticals, Leverkusen, Germany). Images were analyzed using Osirix.

Drug treatment of mice—Stock solutions of ruxolitinib and trametinib were prepared in DMSO and dissolved in 0.5% (w/v) methylcellulose and 0.1% (v/v) Tween-80 in PBS (vehicle). Mice were treated one week after tumor cell injection by oral gavage daily for 3

weeks (subcutaneous model) and 6 weeks (orthotopic model) with vehicle or with ruxolitinib or/and trametinib at 90 mg/kg and 0.1 mg/kg, respectively. In experiments that combined ruxolitinib and trametinib with chemotherapy, mice were treated 5 weeks after tumor cell injection with either etoposide alone (10 mg/kg given i.p. 3 times a week) or in combination with ruxolitinib (60 mg/kg, twice per day) and trametinib (3 mg/kg daily) for 2 weeks

Patient-derived samples—Patient-derived tumor tissue sections were obtained from paraffin-embedded tumor samples under the Children's Oncology Group protocol ANBL-00B1 by H.S. Written informed consent from individuals/parents/guardians were obtained at individual institutions at the time of study enrollment. The study was approved by the CHLA Institutional Review Board under CCI-11-00262 – Neuroblastoma Pathology) which follows the Belmont Report and the U.S. Common Rule

Gene-expression Data

Neuroblastoma Affymetrix Human Exon Array data of 219 primary tumor specimens from patients with high-risk disease were obtained through the NCI Therapeutically Applicable Research to Generate Effective Treatments (TARGET) Consortium (see https://ocg.cancer.gov/programs/target/research). Data were normalized by quantile normalization and summarized using robust multichip average (Affymetrix Power Tools software package, version 1.12). The transcript level data of core probe sets for each sample were averaged based on gene symbol annotations provided by the manufacturer (17,422 unique genes). Spearman correlation analysis between αFAP, FSP-1 and CD163 and was performed on all samples and stratified by MYCN status.

Statistical Analysis

A two-sided unpaired Student's t-test was used to evaluate statistically significant differences between any two groups, whereas multiple group comparisons were performed by 2-way ANOVA. Results were expressed as the mean ± SD of triplicate samples. A p value of less than 0.05 was considered statistically significant. Nonlinear regression of inhibitory dose-response analysis was used to calculate the IC_{50} for etoposide and melphalan. The event-free survival (EFS) curves were calculated by the Kaplan-Meier estimator. The GraphPad Prism version 6.00 for Windows (GraphPad Software Inc., San Diego; www.graphpad.com) was used for the statistical analysis. Experiments were repeated at least twice. For the orthotopic experiment, the area under the curve (AUC) was calculated using the bioluminescence data up to day 55. Mice that did not have measurements for the entire period were considered to have censored AUC measurements. Interval regression was utilized to examine differences in the calculated AUC between treatment groups. Linear regression was used to examine differences in survival time among the different groups in the cohort of mice that showed evidence of tumor growth.

RESULTS

CAF Isolated from Patients with NB Share Characteristics with MSC and are Present in NB Tumors

To study the contribution of CAF to the TME of NB tumors, we isolated CAF from NB tumors obtained at the time of surgical resection. In three out of six tumor samples (Supplementary Table B), we were able after elimination of diasylganglioside (GD2)-positive tumor cells to culture a population of adherent cells, which was positive for the expression of αFibroblast Activation Protein/Dipeptidyl Peptidase IV (αFAP/DPPIV) (Fig. 1A). These cells uniformly expressed other markers of CAF, such as Fibroblast Specific Protein-1 (FSP-1/S1004A) and Vimentin, and had variable expression of αSmooth Muscle Actin (αSMA) (Fig. 1B).

We then compared these cells with MSC isolated from the BM of patients with NB. We demonstrated by flow cytometry that NB-derived CAF have a cell surface marker profile closely related to the profile of BM-MSC (Fig. 1C and Supplementary Fig. S1A). CAF expressed mesenchymal markers such as CD73, CD90 and CD105 (17), but did not express markers of hematopoietic stem cells (CD34), myeloid cells (CD45 and human leukocyte antigen D-related), monocytes (CD14), B-cells (CD19) or endothelial cells (CD31 and VEGFR2).

We then examined whether these NB-derived CAF, like BM-MSC, maintained their pluripotency. In contrast to normal human skin fibroblasts (Fb), but similarly to BM-MSC, CAF retained their ability to differentiate into adipocytes accumulating lipids, osteocytes forming a mineralized matrix and chondrocytes generating a matrix rich in glycosaminoglycans (Fig. 1D and Supplementary Fig. S1B, and Supplementary Fig. S2A).

Altogether, these data identify a new population of CAF that have the phenotypic and functional characteristics of BM-MSC in primary human NB tumors. Thus, we designated these cells CAF-MSC.

To confirm the presence of CAF in primary NB tumors, we then examined the expression of αFAP and FSP-1 in 11 NB specimens by immunohistochemistry. αFAP- and FSP-1-positive cells were identified predominantly in the stromal compartment of the tumors surrounding nests of tumor cells, but were also seen among tumor cells (Fig. 1E). Because we recently reported the presence of TAM in high risk NB tumors (18), we examined some of these primary tumors for the co-presence of CAF and TAM by immunofluorescence. The data revealed the presence of CD163 expressing TAM in close proximity to CAF, suggesting that these two cell types could interact to contribute to the TME in NB (Supplementary Fig. S2B). Additional evidence supporting such association was obtained by a transcriptomic meta-analysis of αFAP and FSP-1 expression in a cohort of 219 tumor samples obtained from patients with high-risk NB. This analysis revealed a statistically significant correlation between the expression of CAF makers and the presence of CD163 TAM both in MYCN amplified and MYCN non-amplified tumors (Fig. 1F and Supplementary Fig. S2C).

CAF-MSC Increase Tumor Engraftment and Growth in Xenograft Models, Mirroring BM-MSC

To understand the function of CAF-MSC in the TME of NB, CAF-MSC or BM-MSC were subcutaneously co-injected with Firefly Luciferase-expressing CHLA-255 cells (CHLA-255-FLuc) in immunodeficient NOD/SCID mice (Fig. 2). The effect on tumor engraftment and growth was monitored by bioluminescence and compared to engraftment and growth of NB cells injected alone. Co-injection of NB cells with Fb was also done as control for MSC. When NB cells were injected alone, tumor engraftment was observed in only 20% of the cases. In contrast, when co-injected with CAF-MSC or BM-MSC (NB:CAF-MSC ratio of 4:1), engraftment reached 100% (Fig. 2A–C). These tumors grew faster (Fig. 2D–E) and led to a significantly shorter overall survival of the mice ($p=0.0001$; Fig. 2F). Co-injection of NB cells and Fb had a stimulatory effect on tumor engraftment and growth, but to a lesser extent. We also tested different NB:CAF-MSC ratios of 4:2 and 4:0.5 in NSG mice. These experiments (Supplementary Fig. S3A–E) demonstrated an enhanced effect on tumor growth with a higher proportion of CAF-MSC (4:2 ratio) and a lower effect with less CAF-MSC (4:0.5 ratio). However even at such lower ratio, the co-injection of CAF-MSC resulted in a 100% tumorigenicity, indicating that even when representing 1/8 of the tumor cell population, CAF-MSC can potentiate tumorigenesis.

To further evaluate the effect of CAF-MSC on the growth of NB cells, an immunohistochemistry analysis was performed to detect Ki-67. A statistically significant increase in Ki-67-positive cells was observed in tumors derived from the co-injection of NB cells with CAF-MSC or BM-MSC, compared to tumors formed by injection of NB cells alone (Fig. 2G), which is consistent with stimulation of proliferation. Fb also increased the percentage of Ki-67 expression, but to a lesser degree. These data indicate that CAF-MSC, like BM-MSC, promote NB tumor engraftment and growth.

CAF-MSC Increase the Viability of NB Cells by Stimulating Proliferation and Inhibiting Apoptosis

The increase in Ki-67 expression in tumors implanted with CAF-MSC suggested an effect of CAF-MSC on tumor cell proliferation. We thus examined this effect in co-cultures of NB-FLuc cells grown in direct contact with CAF-MSC. Indeed CAF-MSC, similarly to BM-MSC, significantly increased the viability of NB cells over time when compared to NB cells cultured alone or co-cultured with Fb (Fig. 3A). This activity, however, did not require cell-cell contact as a similar increase in viability was observed when NB cells were cultured with CAF-MSC or BM-MSC separated by a porous transwell insert (Fig. 3B) or in the presence of the conditioned medium (CM) of co-cultures of NB and CAF-MSC or BM-MSC cells (NB/CAF-MSC and NB/BM-MSC CM) (Fig. 3C). Similar effects were observed with other preparations of CAF-MSC or BM-MSC (Supplementary Fig. S4A). These data indicate that CAF-MSC, as BM-MSC, increase the growth of tumor cells by a mechanism that does not require direct cell-cell contact.

Consistent with the increase in Ki-67 expression found in xenografted tumors, we observed in the case of CHLA-255 cells an increase in the percentage of NB cells in S-phase from 25% in the presence of NB CM or 33.4% in the presence of NB/Fb to 37.6% and 42.6% in

the presence of NB/CAF-MSC CM and NB/BM-MSC CM respectively (Fig. 3D). The difference between NB CM and NB/Fb CM, although smaller, was nevertheless statistically significant, suggesting that normal Fb can be educated by NB cells. We also observed a reduction in the percentage of apoptotic cells in NB cells from 20.1% and 17.0% in the presence of NB CM or NB/Fb CM to 6.7% and 8.1% in the presence of NB/CAF-MSC or NB/BM-MSC CM, respectively (Fig. 3E). Similar observations were made with SK-N-SH cells. Thus, MSC enhance the viability of NB cells not only by increasing proliferation but also by decreasing apoptosis.

CAF-MSC Protect Tumor Cells from Drug-induced Apoptosis

We next investigated whether CAF-MSC could contribute to chemoresistance. For these experiments, we selected two drug-sensitive (CHLA-255 and SK-N-SH) and two drug-resistant (SK-N-BE2 and CHLA-90) NB cell lines and tested the effect of NB/CAF-MSC CM on NB cell viability in the presence of cytotoxic drugs comparing with NB/BM-MSC CM. Dose-response curves for CHLA-255 cells in the presence of etoposide (Fig. 4A) or melphalan (Fig. 4B) revealed a significantly ($p=0.0002$) higher cell viability and an increase in the half maximal inhibitory concentration (IC_{50}) in the presence of NB/CAF-MSC or NB/BM-MSC CM compared to NB CM or NB/Fb CM. A similar observation was made with the drug-sensitive cell line SK-N-SH. In contrast, no effect was observed in the drug-resistant cell lines SK-N-BE(2) and CHLA-90. Similar effects were seen with other preparations of CAF-MSC and BM-MSC (Supplementary Fig. S4B). Consistent with a protective effect of CAF-MSC and BM-MSC on drug-induced apoptosis, we observed a significant reduction ($p=0.003$) of the percentage of apoptotic cells in the presence of etoposide when drug-sensitive NB cells were exposed to NB/CAF-MSC or NB/BM-MSC CM (Fig. 4C). This effect was associated with a decrease in the cleavage of caspase 3 and in caspase 3/7 activity with the chemosensitive cell lines but not with the chemoresistant lines (Fig. 4D–E).

Altogether, these data indicate that CAF-MSC share with BM-MSC a protective effect on drug-induced apoptosis.

The Pro-tumorigenic Activity of CAF-MSC is STAT3- and ERK1/2-dependent

To understand the mechanism underlying the pro-tumorigenic effects of CAF-MSC, we examined the downstream signaling in NB cells exposed to NB/CAF-MSC or NB/BM-MSC CM using a PathScan Intracellular Signaling assay (Fig. 5A and Supplementary Fig. S5A). A rapid increase in the phosphorylation of STAT3 (14 fold), ERK1/2 (8 fold) and STAT1 (7 fold) and of the survival-regulatory proteins PRAS40 (3 fold), Bad (2 fold) and GSK-3B (1,5 fold) was observed in NB cell lines exposed to NB/CAF-MSC CM or NB/BM-MSC. The increase in the phosphorylation of STAT3, ERK1/2 and STAT1 was also observed in NB cells exposed to NB/Fb CM, but was less pronounced (3 fold, 2 fold and 2 fold, respectively). The increase in p-STAT3 and p-ERK1/2 was confirmed by Western blot analysis, demonstrating a rapid and sustained activation of STAT3 and ERK1/2 in NB cells exposed to NB/CAF-MSC and NB/BM-MSC CM (Supplementary Fig. S5B). Furthermore, the increased phosphorylation of STAT3 and ERK1/2 was also demonstrated in NB tumors from mice xenografted subcutaneously with NB cells and CAF-MSC or BM-MSC (Fig. 5B),

compared with tumors derived from the implantation of NB cells alone or of NB cells with Fb.

To test whether STAT3 and/or ERK1/2 activation contribute to the pro-tumorigenic activity of CAF-MSC, we performed experiments with CHLA-255 cells in the presence of ruxolitinib, a small molecule inhibiting JAK2/STAT3, and trametinib, an inhibitor of MEK/ERK1/2 (19,20). A dose-response curve for these drugs indicated an IC_{50} of 6.2 and 1.9 μM for ruxolitinib and trametinib respectively (Fig. 5C). At a concentration lower than the IC_{10} (2.5 μM ruxolitinib and 0.01 μM trametinib), each inhibitor completely blocked the phosphorylation of STAT3 and ERK1/2 respectively, whereas their combination blocked the phosphorylation of both proteins in NB cells exposed to NB/CAF-MSC CM (Fig. 5D). The combination of both inhibitors completely suppressed the stimulatory effects of NB/CAF-MSC and NB/BM-MSC CM on cell proliferation (Fig. 5E and Supplementary Fig. S5C) and restored the sensitivity of NB cells to etoposide (Fig. 5F), whereas each inhibitor had only a partial effect when used alone.

To explore the soluble factors present in the CM of co-cultures of NB cells and CAF-MSC and BM-MSC involved in the activation of STAT3 and ERK1/2, we used a Cytokine Array. This experiment identified, among 36 inflammatory proteins, seven proteins whose concentrations were elevated in the CM of CAF-MSC and BM-MSC as well as in the CM of NB/BM-MSC or NB/CAF-MSC but not in the CM of NB alone. These included MCP-1/CCL2, CXCL1/GROα, CXCL12/SDF-1, ICAM-1/CD45, IL-6, IL-8 and Serpin E1/PAI-1 (Fig. 5G and Supplementary Fig. S6A).

The absence of these factors in the CM of NB alone suggest (but does not demonstrate at this point) that MSC are the main source of their production. We had previously shown that the expression of IL-6 in BM-MSC is increased upon exposure to NB cells (21) and that IL-6 is not produced by NB cells (22). We thus explored whether IL-6 was the cytokine responsible for the upregulation of STAT3, a known down-stream target of IL-6 (23) by performing experiments in the presence of a neutralizing antibody against IL-6 or IL-6 receptor (IL-6R). These experiments (Supplementary Fig. S6B) demonstrated that blocking IL-6 or its receptor, prevented the activation of STAT3 in NB cells treated with IL-6 and sIL-6R but not by the CM of NB/CAF-MSC or NB/BM-MSC, clearly indicating that other soluble factors present in the CM play an important role in activating STAT3 and ERK1/2.

Taken together, these data demonstrate that the pro-tumorigenic activity of CAF-MSC as well as BM-MSC is dependent on STAT3 and ERK1/2 activation in NB cells.

Combined Inhibition of STAT3 and ERK1/2 Impairs the Pro-tumorigenic Activity of CAF-MSC and Sensitizes NB cells to Chemotherapy in Xenograft Models

The effect of STAT3 and ERK1/2 inhibition was then tested on the pro-tumorigenic activity of BM- and CAF-MSC in xenotransplanted mice. We performed a first experiment in NSG mice xenografted subcutaneously with NB cells alone or NB cells mixed with BM-MSC and treated with vehicle or a combination of ruxolitinib and trametinib. Whereas the presence of BM-MSC increased tumor engraftment from 60% (3/5 mice) to 100% (5/5 mice), engraftment was reduced to 40% (2/5 mice) in mice treated with ruxolitinib and trametinib

(Fig. 6A–B). There was also a significant ($p<0.0001$) decrease in tumor growth over time in mice treated with ruxolitinib and trametinib as documented by tumor size and bioluminescence measurements (Fig. 6C and Supplementary Fig. S7A) and a corresponding reduction in the percentage of Ki-67-positive cells in tumor sections (Fig. 6D and Supplementary Fig. S7B). This was also associated with a decrease in p-STAT3 and p-ERK1/2 in tumors from mice treated with the combination of inhibitors (Fig. 6E and Supplementary Fig. S7C), demonstrating that these inhibitors blocked the activation of these pathways *in vivo*.

We then performed experiments with CAF-MSC implanted with NB cells in the sub-renal capsule of NSG mice which were then treated with ruxolitinib, trametinib or their combination, and monitored for survival (Fig. 6F). In this experiment, in the absence of ruxolitinib and trametinib, there was no difference in survival between orthotopic tumors derived from the implantation of NB cells alone or from NB cells co-injected with CAF-MSC. However there was a significant difference in the mean survival time in mice xenografted with NB and CAF-MSC and treated with ruxolitinib and trametinib (82.6 ± 4.6 days) compared with untreated mice xenografted with NB cells alone (59.7 ± 4.6 days; $p=0.001$) or with NB cells and CAF-MSC (56.9 ± 4.46 days; $p<0.001$). The combination also significantly increased survival when compared with trametinib alone ($p=0.027$) but not with ruxolitinib alone ($p=0.269$). Mice treated with ruxolitinib alone also had a mean survival time that was significantly longer (76.1 ± 4.37 days) than mice xenografted with NB cells alone ($p=0.011$) or with NB and CAF-MSC ($p=0.004$). An increase in mean survival time was also observed in mice treated with trametinib alone (69.1 ± 4.61 days) compared with mice xenografted with NB cells alone ($p=0.128$) or NB and CAF-MSC ($p=0.054$), but the effect was not statistically significant. An analysis of the bioluminescence measurements up to day 55 (Fig. 6G–H) revealed a trend toward a lower activity in the group of mice treated with the combination of trametinib and ruxolitinib (Area Under the Curve (AUC) of 223.4 ± 102) compared to untreated mice co-injected with NB cells and CAF-MSC, however this difference was not statistically significant ($p=0.077$).

We then asked whether the combination of ruxolitinib and trametinib would enhance the response of NB tumors to chemotherapy. NSG mice injected in the sub-renal capsule with NB cells alone or mixed with CAF-MSC were treated (5 weeks after injection) for 2 weeks with etoposide alone or in combination with ruxolitinib and trametinib, and monitored for tumor growth and survival. This experiment (Fig. 7A–C) demonstrated that the combination of ruxolitinib and trametinib resulted in a better response to etoposide, as demonstrated by the bioluminescence at day 47 ($p<0.01$) and MRI analysis at day 49. The addition of ruxolitinib and trametinib to etoposide, also increased survival when compared to etoposide alone ($p=0.0001$) (Fig. 7D). We also observed a decrease in p-STAT3 and p-ERK1/2 in tumors from mice treated with the combination of inhibitors (Fig. 7E).

However, as in the previous experiment, we did not observe a significant difference in tumor growth and survival between mice injected with human CAF-MSC and NB cells and mice injected with NB cells alone. We would have anticipated that mice injected with NB alone would have smaller tumors and would survive longer and that the addition of ruxolitinib and trametinib would enhance response to etoposide. We considered the possibility that in this

orthotopic model, tumors could be infiltrated with murine CAF-MSC and thus examined tumors for the presence of murine FSP-1 positive cells. This analysis revealed the presence of FSP-1 positive CAF in the tumor stroma that were not detected in tumors generated by subcutaneous injections of tumor cells (Fig. 7F–G).

Taken together, these data demonstrate that blocking STAT3 and ERK1/2 activation suppresses the pro-tumorigenic activity of CAF and BM-MSC and sensitizes NB tumors to chemotherapy. We thus conclude that in the orthotopic sub-renal model, murine CAF are recruited, activate STAT3 and ERK1/2 and induce drug resistance.

In summary, our data point to a type of CAF that share functional properties of BM-MSC and that via STAT3 and ERK1/2 activation and exert a pro-tumorigenic function. They also suggest that by blocking the signaling pathways, they activate in tumor cells therapeutic response.

DISCUSSION

The isolation from primary NB tumors of a new population of CAF with the phenotypic and functional characteristics of BM-derived MSC brings new insights into the heterogeneous nature of CAF and into their origin. Initially considered as a homogenous population of stromal cells, CAF are in fact a heterogeneous group of stromal cells in the TME (3,24), and their molecular characterization and functions are still a matter of debate. Although αFAP and FSP-1 are two main markers of CAF, they can be expressed by other types of cells. αFAP is expressed in mesodermal cells and fibroblasts in wound tissues (25), and FSP-1 is found in epithelial cells undergoing epithelial to mesenchymal transition and in macrophages (26). The presence of these cells in NB has not been previously reported. αSMA is another marker of CAF, which have the phenotypical and functional properties of myofibroblasts (27), and have recently been shown to exert an anti-tumorigenic activity through their contribution to fibrosis and stimulation of an immune response in pancreatic ductal adenocarcinoma (28). αSMA-positive fibroblasts are present in the more aggressive NB tumors and their presence inversely correlates with the presence of Schwann cells seen in the more benign ganglioneuroblastoma (29). Here, we report a different type of CAF, which in addition to αFAP and FSP-1 and variable expression of αSMA, also expresses molecular markers of MSC such as CD73, CD90 and CD105, and maintains the ability to differentiate into adipocytes, osteocytes and chondrocytes, properties typically associated with MSC (17).

Mishra *et al.* have shown that human BM-MSC from healthy donors can differentiate into αSMA- and FSP-1-expressing CAF when exposed to the conditioned medium of tumor cells, suggesting that BM-MSC are a source of CAF (9). In tumor-bearing mice transplanted with enhanced green fluorescent protein (EGFP) labeled BM, Kidd *et al.* have shown the presence of EGFP-positive CAF expressing αFAP and FSP-1, further supporting a BM origin. In contrast, αSMA, NG2 and CD31 positive cells were found to originate from the surrounding adipose tissues (30). Our data suggest, this time in human tumors, that CAF might originate from the BM. Furthermore, we show that CAF-MSC, although having the characteristics of CAF, maintain the pluripotent function of BM-MSC.

Our systematic comparison with BM-MSC obtained from patients with NB demonstrates that CAF-MSC share the *in vitro* and *in vivo* pro-tumorigenic function of BM-MSC. To the best of our knowledge, the present study is the first to report the presence of such cells in primary human NB tumors. Although these cells were present in all tumors examined by immunohistochemistry, their isolation from fresh human tumors was only successful in 50% of the cases. This may be due to the fact that tumors were obtained from patients after initial treatment with chemotherapy. Tumors were high-risk neuroblastoma tumors and had an unfavorable histology according to the International Neuroblastoma Pathology Classification (31). All three CAF-MSC and all four BM-MSC Isolated share similar phenotypes, abilities to differentiate and pro-tumorigenic functions.

We also demonstrate the presence of αFAP and FSP-1 expressing cells in primary NB tumors by a combination of transcriptomic analysis and immunohistochemistry. These studies provide evidence for an association between CAF and TAM in high-risk NB tumors as the expression of αFAP and FSP-1 correlated with that of CD163, a M2 macrophage marker (4). Although as previously discussed, neither αFAP nor FSP-1 are entirely specific to CAF. We demonstrated by double immunofluorescence staining that FSP-1 expressing cells are different from CD163 expressing cells. The observation that αFAP and FSP-1 expressing cells correlated with that of CD163 expressing cells suggests that these two cell types cooperate in creating a pro-tumorigenic TME. TAM have been shown to be more abundant in metastatic NB tumors and in high-risk NB tumors in patients older than 18 months (18) and the co-presence of CAF and TAM in NB tumors with an unfavorable histological type and poor clinical outcome has been recently reported (32).

A unique aspect of our studies is the use of CAF-MSC and BM-MSC isolated from patients with NB. As a result, we had to use immunodeficient mice for the *in vivo* co-injections with human NB cells. Our experiments thus demonstrate that the pro-tumorigenic effect of CAF-MSC and BM-MSC described here is independent of the immune system. Whether CAF-MSC would have a similar pro-tumorigenic effect in the presence of an intact immune system was not investigated here; however, considering the known immunosuppressive effect of MSC (33,34), one would anticipate an even stronger pro-tumorigenic effect in immunocompetent mice.

Our data demonstrate that when conditioned by tumor cells, CAF-MSC exert a broad spectrum of pro-tumorigenic activities against tumor cells that include a stimulation of proliferation by enhancing entry into S-phase of the cell cycle *in vitro* and *in vivo*, an inhibition of apoptosis and the induction of resistance to chemotherapeutic agents as etoposide and melphalan in drug-sensitive tumor cells *in vitro* and *in vivo*, a resistance mechanism described as environment-mediated drug resistance (EMDR) (35). Etoposide is a topoisomerase inhibitor and melphalan an alkylating agent that inhibits DNA synthesis and RNA synthesis. Both drugs are used in the treatment of patients with NB (36).

As indicated by our data, such resistance to these chemotherapeutic agents was seen in drug-sensitive cells and not in drug-resistant cells and was reversible. The fact that we observed some effect in the presence of human skin fibroblasts used as controls is not unanticipated as tumor cells have the ability to “educate” normal dermal fibroblasts toward a pro-tumorigenic

behavior (37) and all cells in these experiments were pre-conditioned by tumor cells. However, our data clearly indicate that both BM-MSC and CAF-MSC have a much more robust pro-tumorigenic response than skin fibroblasts in the presence of NB cells.

The pro-tumorigenic activities of stromal cells can be exerted by soluble factor-mediated and cell adhesion-mediated mechanisms (35). In the case of NB, we show that the pro-tumorigenic activity of MSC is present in the CM and does not require cell-cell contact, pointing toward a soluble factor-mediated mechanism. We identified several cytokines and chemokines whose concentration was elevated in the CM of CAF-MSC, BM-MSC and the CM of their co-culture with NB cells but not in the CM of NB cells alone. These soluble factors all have a pro-tumorigenic activity, either directly by promoting growth and survival in tumor cells (CXCL1, IL-6), their homing in the bone marrow (SDF-1), and inhibiting cell adhesion (soluble ICAM), or indirectly by promoting angiogenesis (IL-8, PAI-1) or the recruitment of macrophages (MCP-1). Activation of STAT3 by IL-6 has already been reported in NB and other cancer tumors (23,38,39), but by demonstrating that blocking IL-6 or its receptor is not sufficient to block STAT3 activation, the data indicate that other soluble factors than IL-6 present in the CM activate STAT3 and ERK1/2. Although the data do not identify the cellular source of these cytokines, their absence in the CM of NB cells alone suggests a stromal rather than a tumoral origin. In the case of IL-6 and IL-8, we have previously shown by RNA analysis that these cytokines are not produced by NB cells (21). Ultimately it is their increased concentration and activity upon tumor cell-stromal cell interaction rather than their source that is biologically relevant. The data also suggest that targeting a single cytokine or chemokine may have limited therapeutic value in cancer therapy as illustrated in the case of IL-6, where clinical trials targeting this cytokine or its receptor have shown disappointing results (40).

The convergence of the activity of these soluble factors to STAT3 and ERK1/2 signaling pathways in NB cells is consistent with other observations pointing to STAT3 and ERK1/2 in NB. The contribution of STAT3 activation by IL-6 produced by BM-MSC to EMDR has been previously shown by us (23). In a recent genomic analysis comparing relapse and primary NB tumors, activating mutations in the RAS-MAPK pathway were found in 78% of the relapsed NB tumors and these mutations were sensitive to inhibition by MEK inhibitors such as trametinib, cobinetinib or binimetinib (41). Thus, this genomic analysis and our observations suggest that intrinsic (genetic alterations) as well as extrinsic (TME) forces converge toward the hyperactivation of the MAPK pathway in promoting drug resistance in NB tumors.

Our *in vitro* experiments support the concept that simultaneous inhibition of STAT3 and ERK is needed to reverse the stimulatory effect of CAF-MSC and BM-MSC on NB proliferation and drug resistance. The combination of ruxolitinib and trametinib was better than trametinib alone but ruxolitinib was as efficient as the combination. This may be due to differences in pharmacology and pharmacodynamics where trametinib may not have reached optimal tissue concentrations (20). The analysis of bioluminescence also indicated a not statistically significant trend toward a stronger effect of the combination than a single agent alone. This may in part have been due to inherent errors in bioluminescence imaging where

the presence of necrotic and hypoxic areas in large tumors do not efficiently activate luciferin as well perfused tumor tissues do (42).

In a separate experiment, we also observed that a dual inhibition of STAT3 and ERK1/2 pathways decreased tumor growth and increased survival in mice treated with etoposide when compared to etoposide alone supporting our *in vitro* data indicating that STAT3 and ERK1/2 contribute to drug resistance. Interestingly, in these *in vivo* experiments where cells were injected orthotopically in the sub-renal capsule rather than subcutaneously, the addition of human MSC had no significant effect on survival or response to chemotherapy. However we observed the presence of murine FSP-1 positive cells in these tumors and evidence of STAT3 and ERK1/2 activation, and accordingly an improved response with the addition of ruxolitinib and trametinib. This indicates that in the orthotopic model tumors recruit murine CAF-MSC that confer drug resistance whereas they are less able to do so when injected subcutaneously and require exogenous CAF-MSC. Altogether, the data suggest that pharmacological inhibition of STAT3 and ERK1/2 could be a valuable therapeutic approach to enhance response to chemotherapy.

In summary, our data demonstrate the presence in human NB tumors of a new type of CAF that share phenotypic and functional pro-tumorigenic properties of BM-MSC and provide evidence that the pro-tumorigenic activity of these cells is based on their activation of STAT3 and ERK1/2 in tumor cells. Since CAF contribute to the progression of many other cancer types like colon (43), endometrial (44), ovarian (10,45), breast (46), and pancreatic (37) cancers, our observations are relevant to cancers other than NB.

Supplementary Material

Refer to Web version on PubMed Central for supplementary material.

Acknowledgments

Grant Support: This article was supported by grants CA81403 to R.C. Seeger and Y.A. DeClerck and CA163117 to Y.A. DeClerck from the National Institutes of Health, and grant RC1MD004418 from the National Institutes of Health to R.C. Seeger and S. Asgharzadeh. L. Borriello was supported by a Research Career Development Fellowship from The Saban Research Institute of Children's Hospital Los Angeles.

The authors thank J. Rosenberg for her excellent assistance in manuscript preparation, Dr. M. Fabbri for helpful editorial comments, G. Karapetyan for acquisition of the imaging data, and Dr. Martine Torres for editorial assistance.

References

1. Hanahan D, Weinberg RA. Hallmarks of cancer: the next generation. Cell. 2011; 144:646–74. [PubMed: 21376230]
2. Lyden D, Hattori K, Dias S, Costa C, Blaikie P, Butros L, et al. Impaired recruitment of bone-marrow-derived endothelial and hematopoietic precursor cells blocks tumor angiogenesis and growth. NatMed. 2001; 7:1194–201.
3. Ohlund D, Elyada E, Tuveson D. Fibroblast heterogeneity in the cancer wound. J Exp Med. 2014; 211:1503–23. [PubMed: 25071162]
4. Mantovani A, Locati M. Tumor-associated macrophages as a paradigm of macrophage plasticity, diversity, and polarization: lessons and open questions. Arterioscler Thromb Vasc Biol. 2013; 33:1478–83. [PubMed: 23766387]

5. Augsten M. Cancer-associated fibroblasts as another polarized cell type of the tumor microenvironment. Front Oncol. 2014; 4:62. [PubMed: 24734219]
6. Direkze NC, Forbes SJ, Brittan M, Hunt T, Jeffery R, Preston SL, et al. Multiple organ engraftment by bone-marrow-derived myofibroblasts and fibroblasts in bone-marrow-transplanted mice. Stem Cells. 2003; 21:514–20. [PubMed: 12968105]
7. Direkze NC, Hodivala-Dilke K, Jeffery R, Hunt T, Poulsom R, Oukrif D, et al. Bone marrow contribution to tumor-associated myofibroblasts and fibroblasts. Cancer Res. 2004; 64:8492–5. [PubMed: 15574751]
8. Phinney DG, Prockop DJ. Concise review: mesenchymal stem/multipotent stromal cells: the state of transdifferentiation and modes of tissue repair--current views. Stem Cells. 2007; 25:2896–902. [PubMed: 17901396]
9. Mishra PJ, Mishra PJ, Humeniuk R, Medina DJ, Alexe G, Mesirov JP, et al. Carcinoma-associated fibroblast-like differentiation of human mesenchymal stem cells. Cancer Res. 2008; 68:4331–9. [PubMed: 18519693]
10. Spaeth EL, Dembinski JL, Sasser AK, Watson K, Klopp A, Hall B, et al. Mesenchymal stem cell transition to tumor-associated fibroblasts contributes to fibrovascular network expansion and tumor progression. PLoS ONE. 2009; 4:e4992. [PubMed: 19352430]
11. Cheung NK, Dyer MA. Neuroblastoma: developmental biology, cancer genomics and immunotherapy. Nat Rev Cancer. 2013; 13:397–411. [PubMed: 23702928]
12. Borriello L, Seeger RC, Asgharzadeh S, DeClerck YA. More than the genes, the tumor microenvironment in neuroblastoma. Cancer Lett. 2016; 380:304–14. [PubMed: 26597947]
13. Sugiura Y, Shimada H, Seeger RC, Laug WE, DeClerck YA. Matrix metalloproteinases-2 and −9 are expressed in human neuroblastoma: contribution of stromal cells to their production and correlation with metastasis. Cancer Res. 1998; 58:2209–16. [PubMed: 9605768]
14. Bergfeld SA, Blavier L, DeClerck YA. Bone marrow-derived mesenchymal stromal cells promote survival and drug resistance in tumor cells. Mol Cancer Ther. 2014; 13:962–75. [PubMed: 24502925]
15. Schindelin J, Arganda-Carreras I, Frise E, Kaynig V, Longair M, Pietzsch T, et al. Fiji: an open-source platform for biological-image analysis. NatMethods. 2012; 9:676–82.
16. Chantrain CF, Shimada H, Jodele S, Groshen S, Ye W, Shalinsky DR, et al. Stromal matrix metalloproteinase-9 regulates the vascular architecture in neuroblastoma by promoting pericyte recruitment. Cancer Res. 2004; 64:1675–86. [PubMed: 14996727]
17. Horwitz EM, Le Blanc K, Dominici M, Mueller I, Slaper-Cortenbach I, Marini FC, et al. Clarification of the nomenclature for MSC: The International Society for Cellular Therapy position statement. Cytotherapy. 2005; 7:393–5. [PubMed: 16236628]
18. Asgharzadeh S, Salo JA, Ji L, Oberthuer A, Fischer M, Berthold F, et al. Clinical significance of tumor-associated inflammatory cells in metastatic neuroblastoma. J Clin Oncol. 2012; 30:3525–32. [PubMed: 22927533]
19. Pemmaraju N, Kantarjian H, Kadia T, Cortes J, Borthakur G, Newberry K, et al. A Phase I/II Study of the Janus Kinase (JAK)1 and 2 Inhibitor Ruxolitinib in Patients With Relapsed or Refractory Acute Myeloid Leukemia. Clin Lymphoma Myeloma Leuk. 2014
20. Gilmartin AG, Bleam MR, Groy A, Moss KG, Minthorn EA, Kulkarni SG, et al. GSK1120212 (JTP-74057) is an inhibitor of MEK activity and activation with favorable pharmacokinetic properties for sustained in vivo pathway inhibition. Clin Cancer Res. 2011; 17:989–1000. [PubMed: 21245089]
21. Sohara Y, Shimada H, Minkin C, Erdreich-Epstein A, Nolta JA, DeClerck YA. Bone marrow mesenchymal stem cells provide an alternate pathway of osteoclast activation and bone destruction by cancer cells. Cancer Res. 2005; 65:1129–35. [PubMed: 15734993]
22. Ara T, Song L, Shimada H, Keshelava N, Russell HV, Metelitsa LS, et al. Interleukin-6 in the bone marrow microenvironment promotes the growth and survival of neuroblastoma cells. Cancer Res. 2009; 69:329–37. [PubMed: 19118018]
23. Ara T, Nakata R, Sheard MA, Shimada H, Buettner R, Groshen SG, et al. Critical Role of STAT3 in IL-6-Mediated Drug Resistance in Human Neuroblastoma. Cancer Res. 2013; 73:3852–64. [PubMed: 23633489]

24. Kalluri R, Zeisberg M. Fibroblasts in cancer. Nat Rev Cancer. 2006; 6:392–401. [PubMed: 16572188]
25. Jacob M, Chang L, Pure E. Fibroblast activation protein in remodeling tissues. Curr Mol Med. 2012; 12:1220–43. [PubMed: 22834826]
26. Osterreicher CH, Penz-Osterreicher M, Grivennikov SI, Guma M, Koltsova EK, Datz C, et al. Fibroblast-specific protein 1 identifies an inflammatory subpopulation of macrophages in the liver. Proc Natl Acad Sci U S A. 2011; 108:308–13. [PubMed: 21173249]
27. Desmouliere A, Guyot C, Gabbiani G. The stroma reaction myofibroblast: a key player in the control of tumor cell behavior. Int J Dev Biol. 2004; 48:509–17. [PubMed: 15349825]
28. Ozdemir BC, Pentcheva-Hoang T, Carstens JL, Zheng X, Wu CC, Simpson TR, et al. Depletion of carcinoma-associated fibroblasts and fibrosis induces immunosuppression and accelerates pancreas cancer with reduced survival. Cancer Cell. 2014; 25:719–34. [PubMed: 24856586]
29. Zeine R, Salwen HR, Peddinti R, Tian Y, Guerrero L, Yang Q, et al. Presence of cancer-associated fibroblasts inversely correlates with Schwannian stroma in neuroblastoma tumors. Mod Pathol. 2009; 22:950–8. [PubMed: 19407854]
30. Kidd S, Spaeth E, Watson K, Burks J, Lu H, Klopp A, et al. Origins of the tumor microenvironment: quantitative assessment of adipose-derived and bone marrow-derived stroma. PLoSONE. 2012; 7:e30563.
31. Shimada H, Umehara S, Monobe Y, Hachitanda Y, Nakagawa A, Goto S, et al. International neuroblastoma pathology classification for prognostic evaluation of patients with peripheral neuroblastic tumors: a report from the Children's Cancer Group. Cancer. 2001; 92:2451–61. [PubMed: 11745303]
32. Hashimoto O, Yoshida M, Koma YI, Yanai T, Hasegawa D, Kosaka Y, et al. Collaboration of cancer-associated fibroblasts and tumour-associated macrophages for neuroblastoma development. J Pathol. 2016
33. Kraman M, Bambrough PJ, Arnold JN, Roberts EW, Magiera L, Jones JO, et al. Suppression of antitumor immunity by stromal cells expressing fibroblast activation protein-alpha. Science. 2010; 330:827–30. [PubMed: 21051638]
34. Poggi A, Musso A, Dapino I, Zocchi MR. Mechanisms of tumor escape from immune system: role of mesenchymal stromal cells. Immunol Lett. 2014; 159:55–72. [PubMed: 24657523]
35. Meads MB, Gatenby RA, Dalton WS. Environment-mediated drug resistance: a major contributor to minimal residual disease. Nat Rev Cancer. 2009; 9:665–74. [PubMed: 19693095]
36. Gordon SJ, Pearson AD, Reid MM, Craft AW. Toxicity of single-day high-dose vincristine, melphalan, etoposide and carboplatin consolidation with autologous bone marrow rescue in advanced neuroblastoma. Eur J Cancer. 1992; 28a:1319–23. [PubMed: 1515242]
37. Erez N, Truitt M, Olson P, Arron ST, Hanahan D. Cancer-Associated Fibroblasts Are Activated in Incipient Neoplasia to Orchestrate Tumor-Promoting Inflammation in an NF-kappaB-Dependent Manner. Cancer Cell. 2010; 17:135–47. [PubMed: 20138012]
38. Yeh HH, Lai WW, Chen HH, Liu HS, Su WC. Autocrine IL-6-induced Stat3 activation contributes to the pathogenesis of lung adenocarcinoma and malignant pleural effusion. Oncogene. 2006; 25:4300–9. [PubMed: 16518408]
39. Lou W, Ni Z, Dyer K, Tweardy DJ, Gao AC. Interleukin-6 induces prostate cancer cell growth accompanied by activation of stat3 signaling pathway. Prostate. 2000; 42:239–42. [PubMed: 10639195]
40. Rossi JF, Lu ZY, Jourdan M, Klein B. Interleukin-6 as a therapeutic target. Clin Cancer Res. 2015; 21:1248–57. [PubMed: 25589616]
41. Eleveld TF, Oldridge DA, Bernard V, Koster J, Daage LC, Diskin SJ, et al. Relapsed neuroblastomas show frequent RAS-MAPK pathway mutations. Nat Genet. 2015; 47:864–71. [PubMed: 26121087]
42. Dickson PV, Hamner B, Ng CY, Hall MM, Zhou J, Hargrove PW, et al. In vivo bioluminescence imaging for early detection and monitoring of disease progression in a murine model of neuroblastoma. J Pediatr Surg. 2007; 42:1172–9. [PubMed: 17618876]

43. Nakagawa H, Liyanarachchi S, Davuluri RV, Auer H, Martin EW Jr, de la Chapelle A, et al. Role of cancer-associated stromal fibroblasts in metastatic colon cancer to the liver and their expression profiles. Oncogene. 2004; 23:7366–77. [PubMed: 15326482]

44. Subramaniam KS, Tham ST, Mohamed Z, Woo YL, Mat Adenan NA, Chung I. Cancer-associated fibroblasts promote proliferation of endometrial cancer cells. PLoS One. 2013; 8:e68923. [PubMed: 23922669]

45. McLean K, Gong Y, Choi Y, Deng N, Yang K, Bai S, et al. Human ovarian carcinoma-associated mesenchymal stem cells regulate cancer stem cells and tumorigenesis via altered BMP production. J Clin Invest. 2011; 121:3206–19. [PubMed: 21737876]

46. Peng Q, Zhao L, Hou Y, Sun Y, Wang L, Luo H, et al. Biological characteristics and genetic heterogeneity between carcinoma-associated fibroblasts and their paired normal fibroblasts in human breast cancer. PLoS One. 2013; 8:e60321. [PubMed: 23577100]

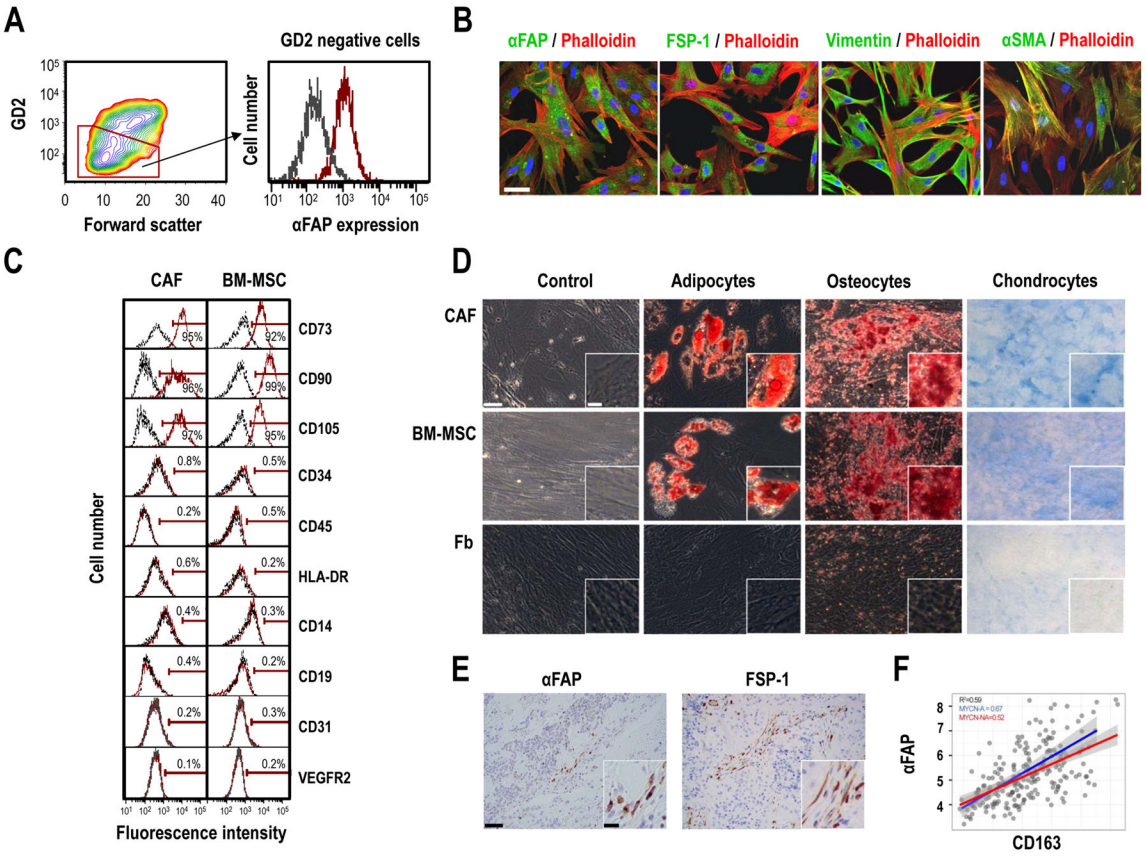

Figure 1. CAF isolated from patients with NB share characteristics with MSC, and are present in primary NB tumors

A: Fluorescence-activated cell sorting (FACS) of a subpopulation of GD2-negative cells expressing αFAP from a freshly digested NB tumor. In the histogram overlay on the right, the black line represents isotype control and the red line represents specific staining; **B:** Representative immunofluorescence images captured by confocal microscopy of CAF-MSC stained for αFAP, FSP-1, Vimentin and αSMA and counterstained with Phalloidin and DAPI. Scale bar = 50 μm; **C:** Expression of surface markers by flow cytometry in cultured CAF-MSC and BM-MSC; **D:** Top: Representative images of CAF-MSC, BM-MSC and Fb differentiated into adipocytes, osteocytes and chondrocytes. Bottom: Histogram representing the quantification of differentiated cells by measuring the absorbance (±SD) of solubilized Oil Red O staining (adipocytes), Alizarin Red (osteocytes) and Alcian Blue (chondrocytes) from duplicate wells. Scale bar = 50 μm in the main picture and 15 μm in insert. **E:** Representative images of sections of NB tumors (n=11) stained for αFAP or FSP-1 as described in Materials and Methods. Scale bar = 50μm in the main picture and 15 μm in insert; **F:** Scatter diagrams of mRNA expression of αFAP and CD163 in primary tumors of children with high-risk NB (n=219). Spearman correlation values and regression lines for the entire dataset and subsets of samples with MYCN-A (blue line) and those with MYC-NA (red line).

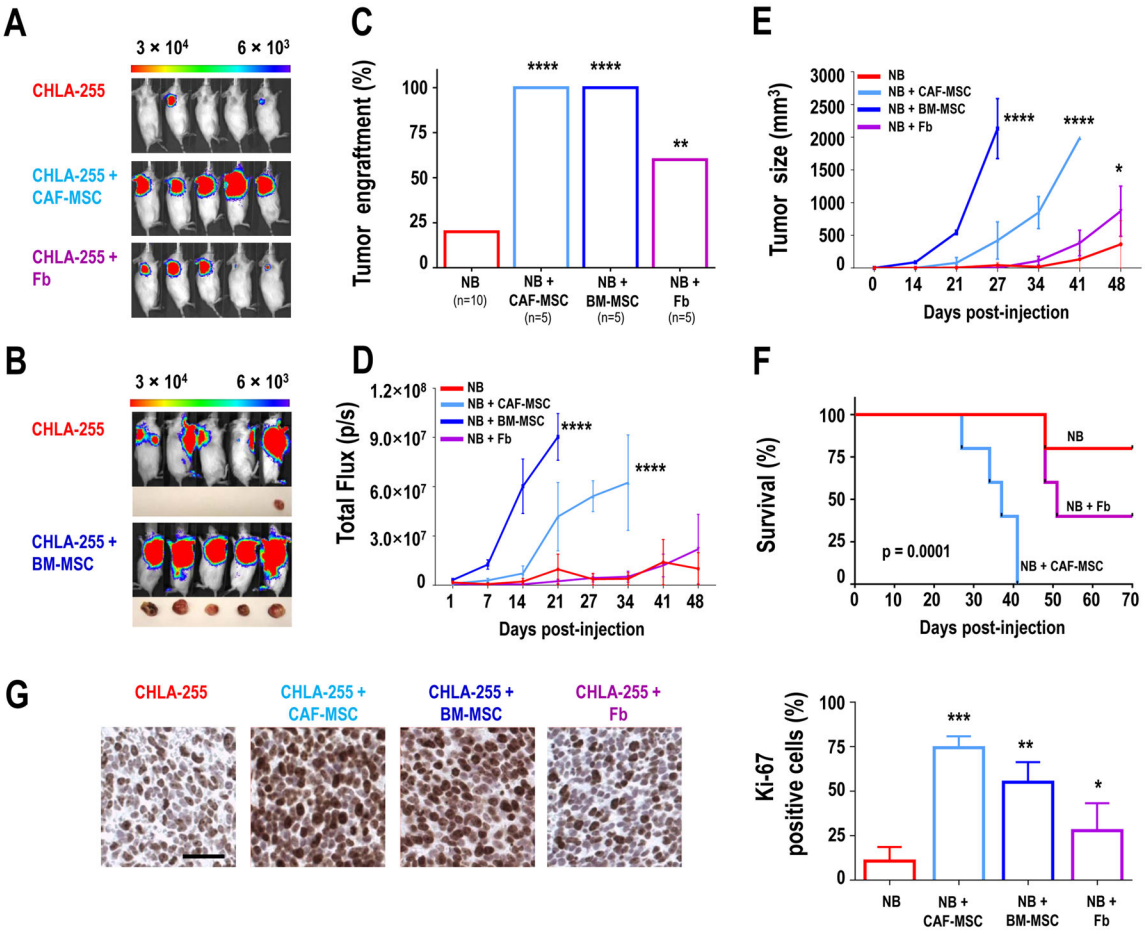

Figure 2. CAF-MSC increase tumor engraftment and growth in xenograft models

A: Representative bioluminescence images of NOD/SCID mice (n=5 per group) taken at day 21 after subcutaneous injection into the right flank of CHLA-255-FLuc cells, either alone or mixed with CAF-MSC or Fb (ratio 4:1); **B**: Representative bioluminescence images of NOD/SCID mice (n=5 per group) taken at day 21 after subcutaneous injection of CHLA-255-FLuc cells alone into the right flank or mixed with BM-MSC into the left flank. Representative pictures of tumors harvested at day 27 are shown below the bioluminescence images. Note that the bioluminescence from the tumor in the left flank remains visible in images taken of the right flank; **C:** Percentage of engrafted tumors in each group for the 2 experiments (A and B); **D:** Average of the bioluminescence signal intensity (p/s = photons per second) over time of all mice (±SEM) in each group; **E:** Average tumor size (±SEM) over time of all mice in each group; **F:** Kaplan-Meier survival curves in each group of mice in experiment shown in **A; G:** Left: Representative images of Ki-67 expression in tumors from each group of mice. Right: Quantification of Ki-67-positive cells (±SEM) from an average of 10 fields (×20) examined for each section in each group. Scale bar = 50 μm; *p<0.05; **p< 0.01, *** for p<0.001, and **** for p< 0.0001.

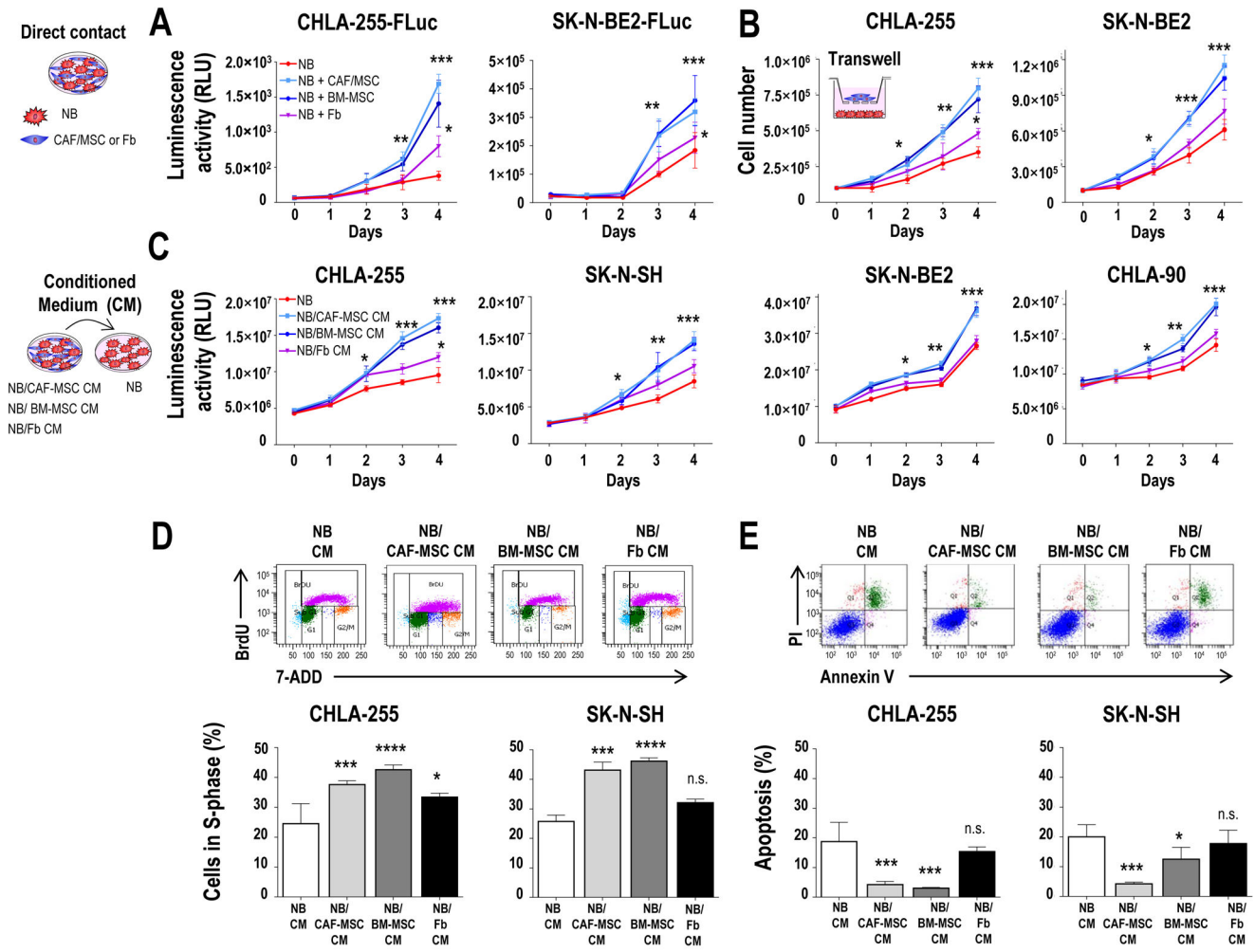

Figure 3. CAF-MSC and BM-MSC promote tumor cell viability by increasing proliferation and inhibiting apoptosis

A: Indicated NB-FLuc cells were cultured in direct contact with CAF-MSC, BM-MSC or Fb (ratio 4:1), and examined for viability over 4 days by adding D-Luciferin as described in Materials and Methods. As controls, NB cells were grown alone in their own conditioned medium. The data represent the mean (±SD) luminescence activity in relative light units (RLU) from six samples and are representative of one of three independent experiments showing similar results; **B:** Indicated NB cells were co-cultured in a transwell system using the same conditions as in **A**. The data represent the mean number (±SD) of trypan blue-negative cells in triplicate samples and are representative of one of two independent experiments showing similar results; **C:** Indicated NB cells were cultured in CM from NB, NB/CAF-MSC, NB/BM-MSC or NB/Fb co-cultures and examined for viability by CellTiterGlo as described in Materials and Methods, over 4 days as in **A**. The data represent the mean (±SD) luminescence activity of six samples and are representative of one of two independent experiments; **D:** Indicated NB cells were cultured as described in **C** and examined for BrdU incorporation after 48 hours as indicated in Materials and Methods. The histograms represent the mean (±SD) percentage of cells in S-phase for triplicate samples

and results are representative of one of three independent experiments showing similar results; **E:** NB cells were cultured as indicated in **C** and examined for apoptosis after 4 days by flow cytometry as indicated in Materials and Methods. The histograms represent the mean (±SD) percentage of Annexin V^+/PI^+ and Annexin V^+/PI^- cells for triplicate samples, and results are representative of one of two independent experiments showing similar results. *p<0.05;**p< 0.01; ***p<0.001; ****p< 0.0001; n.s. = not significant.

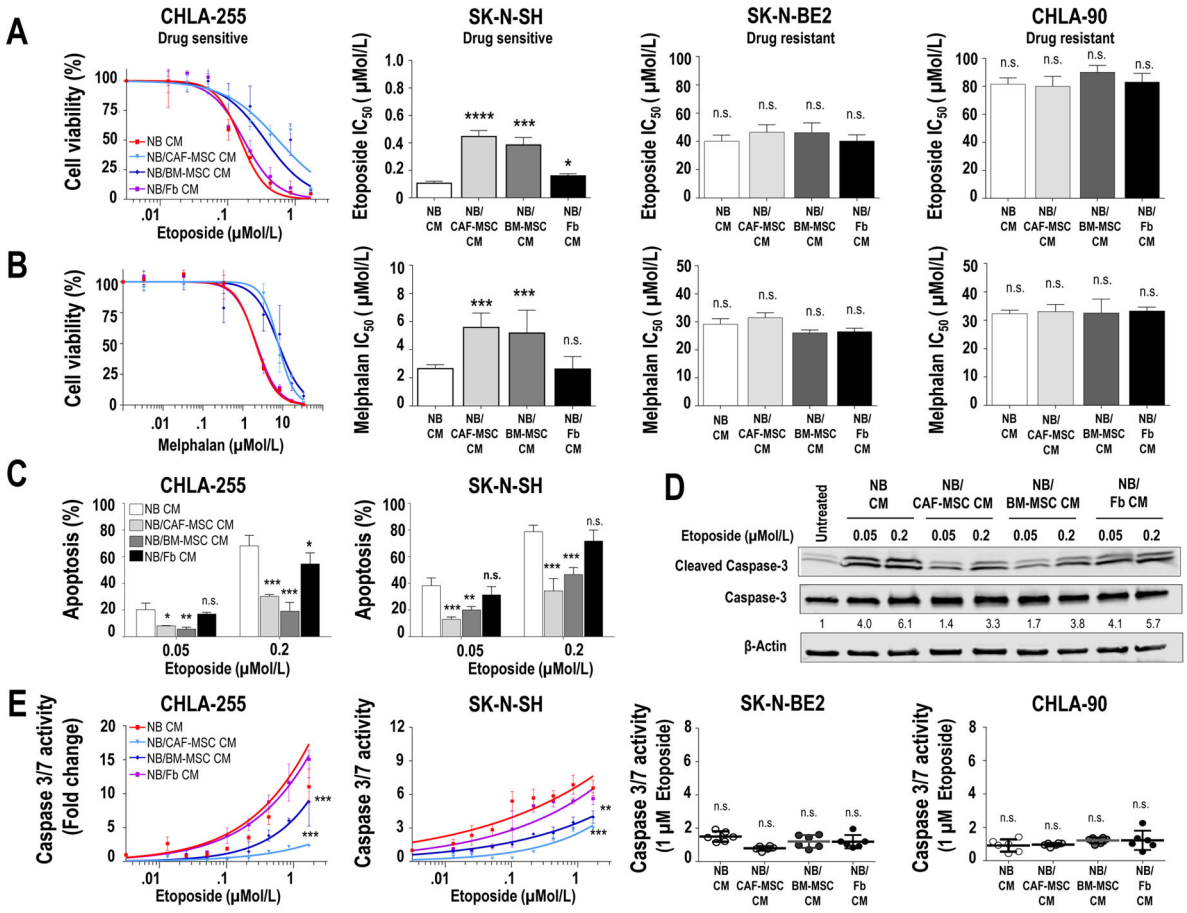

Figure 4. CAF-MSC protect tumor cells from drug-induced apoptosis

A–B: Indicated NB cells were cultured in CM from NB, NB/CAF-MSC, NB/BM-MSC or NB/Fb co-cultures, treated with etoposide (A) or melphalan (B) at the indicated concentrations for 48 hours and examined for cell viability. The graph on the left represents the dose-response curve with the mean (±SD) percentage of viable cells from control (no drug) in triplicate samples and are representative of one of three independent experiments showing similar results. The histograms on the right represent the mean (±SD) IC_{50} values calculated from the dose-response curves; **C:** NB cells were cultured as described in **A**, treated at the indicated concentrations of etoposide, and examined after 48 hours for apoptosis by flow cytometry. The histograms represent the mean (±SD) percentage of Annexin V^+/PI^+ and Annexin V^+/PI^- cells from triplicate samples and results are representative of one of two independent experiments showing similar results; **D:** CHLA-255 cells were cultured and treated as in **C** and examined after 48 hours for cleavage of caspase-3 by western blot analysis. β-actin was used as a loading control; **E:** Indicated NB cells were cultured and treated as described in **A** and examined for caspase 3/7 activity after 48 hours. The data represent the mean fold change (±SD) of caspase 3/7 activity from triplicate samples and are representative of one of two independent experiments showing similar results. The scatter dot plot graphics on the right represent the mean fold change (±SD) of caspase 3/7 activity of NB treated with etoposide at a concentration of 1 μM and

are representative of one of two experiments showing similar results. *p<0.05; **p< 0.01; ***p<0.001; ****p< 0.0001; n.s. = non-significant.

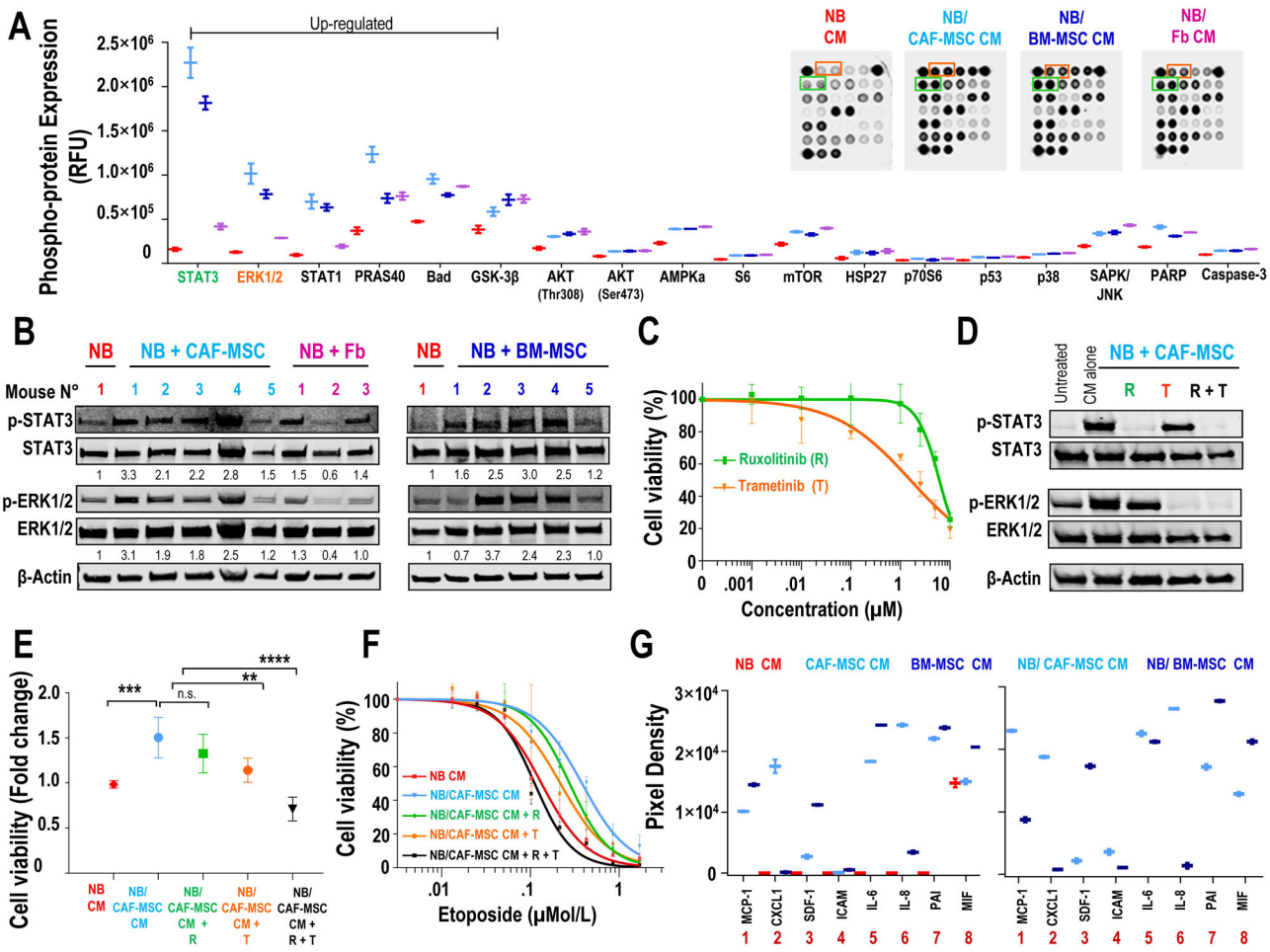

Figure 5. The pro-tumorigenic activity of CAF-MSC is STAT3 and ERK1/2-dependent

A: CHLA-255 cells were exposed to CM from NB, NB/CAF-MSC, NB/BM-MSC or NB/Fb co-cultures for 30 minutes and analyzed for the indicated phosphorylated proteins using the PathScan Intracellular Signaling Array. The graphic represents the mean (±SD) relative fluorescence units (RFU) for each phosphorylated protein. Insert: Picture of typical dot blots; **B:** Western blot analysis of the expression of p-STAT3 and p-ERK1/2 in lysates of tumors obtained from the subcutaneous injection of mice with CHLA-255-FLuc cells alone or mixed with CAF-MSC, Fb or BM-MSC as shown in Fig. 2A–B. β-Actin was used as a loading control; **C:** CHLA-255 cells were treated with increased concentrations of ruxolitinib (R) or trametinib (T) and examined for cell viability after 48 hours. The data represent the mean (±SD) percentage of viable cells determined by the luminescence activity from triplicate samples and results are representative of one of two independent experiments showing similar results; **D:** Western blot analysis of the expression of p-STAT3, STAT3, p-ERK1/2 and ERK1/2 in CHLA-255 cells exposed to NB/CAF-MSC CM and treated with ruxolitinib (2.5 μM), trametinib (0.01 μM) or combination of both inhibitors for 30 minutes. β-Actin was used as a loading control. Data are representative of one of two independent experiments showing similar results; **E:** CHLA-255 cells were exposed to NB CM or NB/ CAF-MSC CM, treated as in **D** and examined for viability after 48 hours. The data represent

the mean (±SD) fold change of cells viability determined by the luminescence activity from triplicate samples and results are representative of one of two independent experiments; **F:** CHLA-255 cells were exposed to NB CM or NB/CAF-MSC CM, treated with the indicated concentrations of etoposide in the presence of ruxolitinib (R), trametinib (T) or their combination (R+T) and examined for viability after 48 hours. The data represent the mean (±SD) percentage of viable cells determined by luminescence activity from triplicate samples and are representative of one of two independent experiments showing similar results. **G:** CHLA-255, CAF-MSC and BM-MSC cells were cultured alone or together for 48 hours. The levels of soluble factors present in the CM were analyzed by a Cytokine Array Panel and quantified by scanning as described in Materials and Methods. The graphs represent the mean (±SD) pixel density of each duplicate spot obtained with CM of cells cultured alone (left) or together (right). **p< 0.01; ***p<0.001; ****p< 0.0001; n.s. = non-significant.

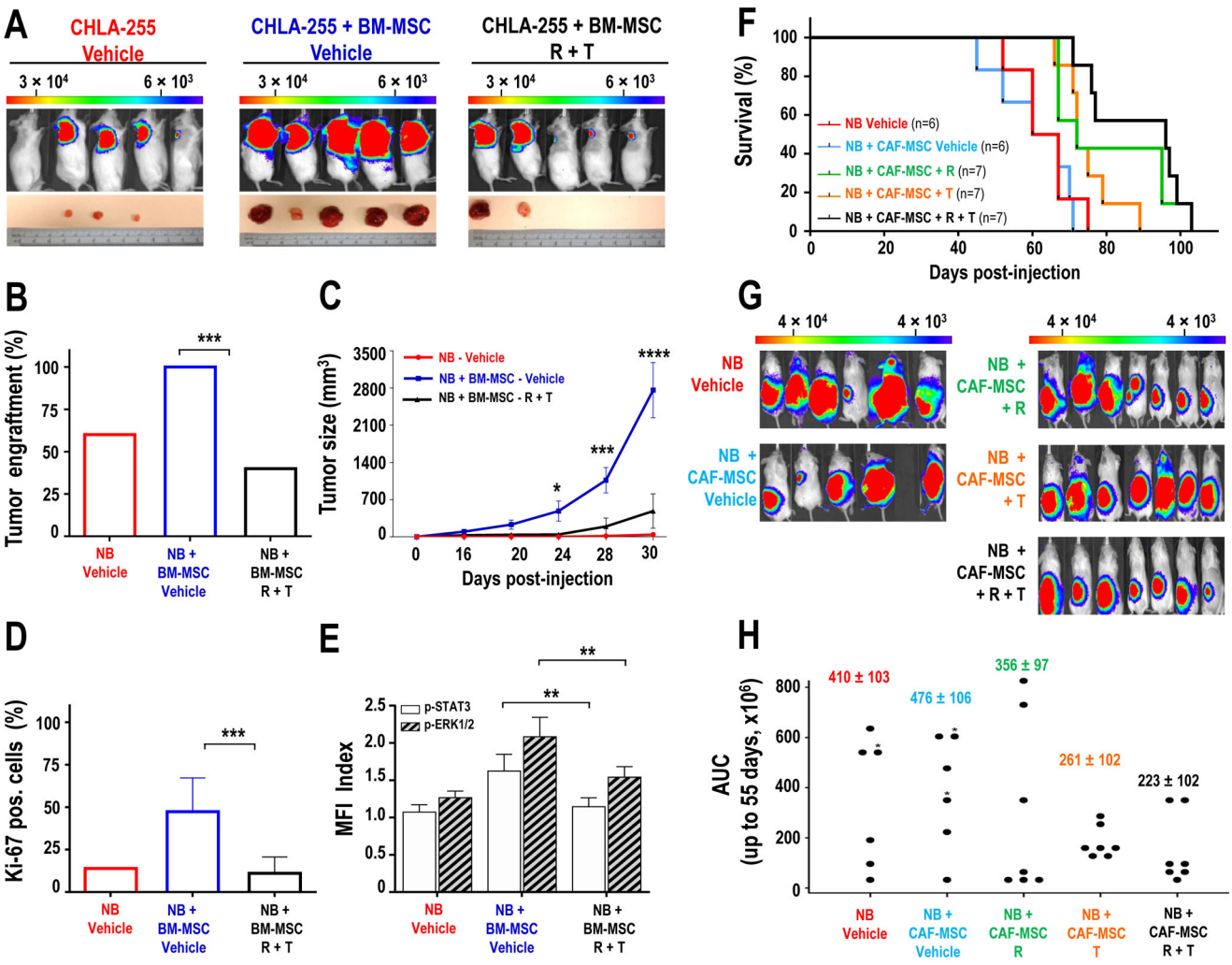

Figure 6. Inhibition of STAT3 and ERK1/2 suppresses tumor engraftment and growth and increases survival in NB xenograft models

A: Representative bioluminescence images of NSG mice at day 30 after subcutaneous injection with CHLA-255-FLuc cells alone (n=5) or mixed with BM-MSC (ratio 4:1) and treated with vehicle (n=5) or ruxolitinib (R, 90 mg/kg/day) and trametinib (T, 0.1 mg/kg/day) (n=5). Lower panel: pictures of tumors harvested at day 32; **B:** Percentage of engrafted tumors in each group; **C:** Mean (±SD) tumor size over time for all mice in each group; **D:** Quantification of Ki-67-positive cells (±SEM) from an average of 10 fields (×20) examined for each section in each group. The data represent the mean (±SD) percent of Ki-67 positive cells from 10 fields (×20) examined for each tumor section; **E:** Flow cytometry analysis for p-STAT3 and p-ERK1/2 in GD2-positive NB cells harvested from tumors shown in **A**. The data represent the mean (±SD) MFI index from all developed tumors in each group; **F:** Kaplan-Meier survival curves of mice injected in the sub-renal capsule with CHLA-255-FLuc cells alone or with CAF-MSC (ratio 4:1). One week after implantation, mice were treated with vehicle or ruxolitinib (R, 90 mg/kg/day), or trametinib (T, 0.1 mg/kg/day), or their combination (R+T). The data are the results of 2 independent experiments with a total of 33 mice that developed tumors. Mice that didn't developed tumors were excluded from

the analysis; **G:** Representative bioluminescence images at day 50 of NSG mice in each group **H:** Dot plot of area under curve (AUC) of all bioluminescence signal intensity (p/s = photons per second) up to day 55 (n=33 mice) in each group. The stars indicate which mouse had a censored AUC as they died before day 55. * $p<0.05$; ** $p< 0.01$; *** $p<0.001$.

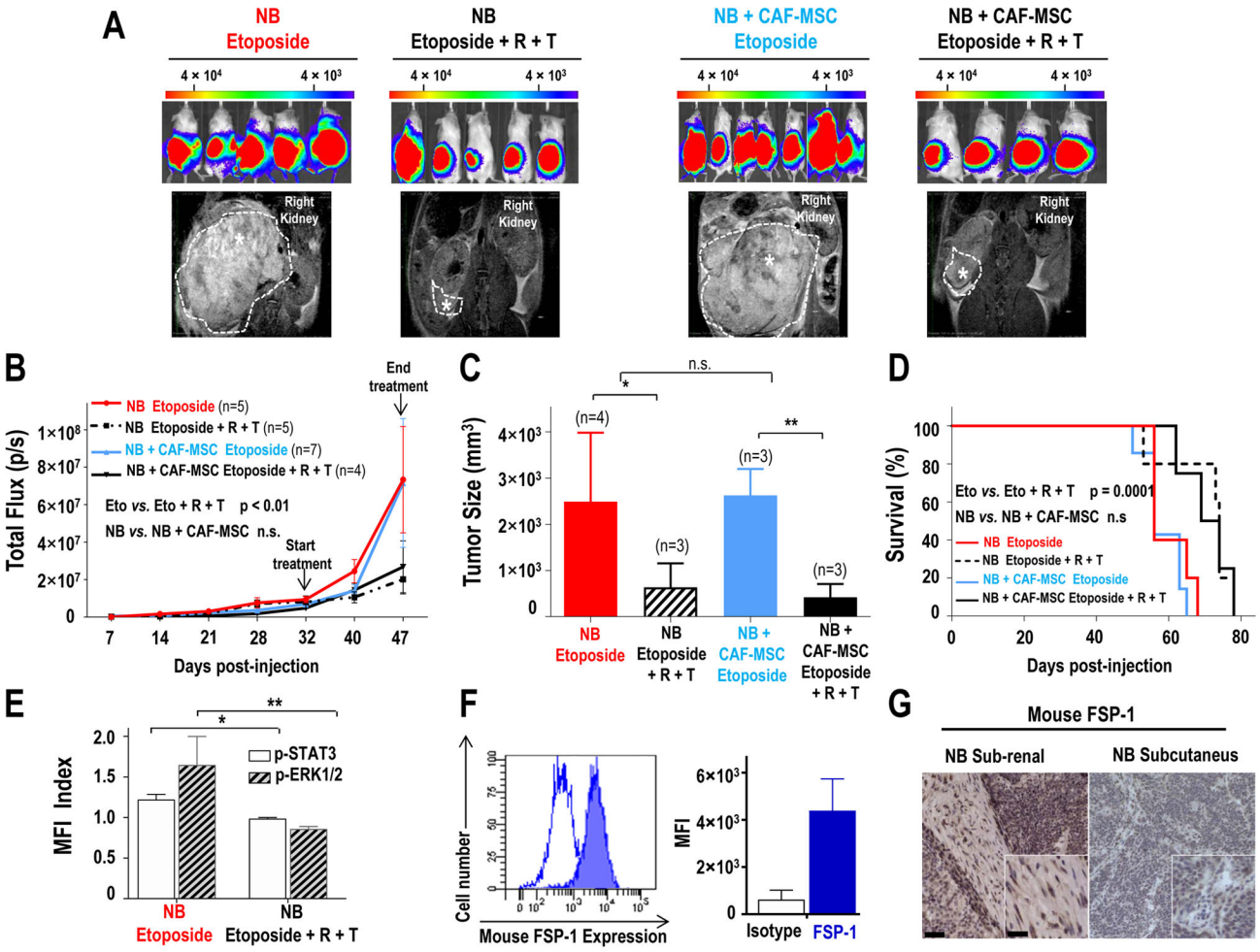

Figure 7. Combined inhibition of STAT3 and ERK1/2 sensitizes NB cells to chemotherapy in xenograft model

A: Representative bioluminescence images of NSG mice at day 47 after sub-renal capsule injection with CHLA-255-FLuc cells alone or mixed with CAF-MSC (ratio 4:1). After five weeks, mice were treated either with etoposide (10 mg/kg, three times/week) or etoposide and a combination of ruxolitinib (R, 60 mg/kg/twice a day) and trametinib (T, 3 mg/kg/day) for two weeks. Lower panel: Representative MRI images of the tumors at day 49; **B:** Average bioluminescence signal intensity (p/s = photons per second) over time of all mice (±SD) in each group; **C:** Average tumor size (±SD) measured by MRI at day 49; **D:** Kaplan-Meier survival curves in each group of mice; **E:** Flow cytometry analysis for p-STAT3 and p-ERK1/2 in GD2-positive NB cells harvested from tumors five hours after treatment with R and T. The data represent the MFI from 2 tumors in each group; **F:** Flow cytometry analysis of mFSP-1 expression in tumors derived from the injection of NB cells alone. Left: Open curve represents the isotype control and the filled curve represents mFSP-1 staining. Right: The histogram represents the MFI (±SD) from three tumors; **G:** Representative images of sections of tumors derived from injection of NB cells alone under the renal capsule or subcutaneously and stained for mouse FSP-1 as described in Materials and Methods. Scale

bar = 50 μm in the main picture and 20 μm in insert. *p<0.05; **p< 0.01; n.s. = not significant.